

Prediction of rivulet transition in anti-icing applications

Anne Gosset*

**University of A Coruña, Department of Naval and Industrial Engineering
Campus de Esteiro, 15403 Ferrol, Spain*

anne.gosset@udc.es

*Corresponding author

Abstract

In this paper, different methods to predict the breakup of a runback water film into rivulets are explored. The Minimum Total Energy criterion is first applied to a sheared film on a NACA profile and confronted to experimental data. The film solver in the CFD code OpenFoam[®] is then used to compute the breakup of a falling film on an inclined plane. The results are substantially dependent on the mesh density and empirical parameters introduced in the partial wetting model. If the later are correctly calibrated for a particular test case, the critical flow rate for transition is well recovered.

1. Introduction

This work deals with the prediction of the breakup of a sheared liquid film into rivulets. It is motivated by the problematics of ice accretion on aircraft components. When an aircraft flies through icing clouds or rain, supercooled water droplets impinge on its wings and form ice if these aerodynamic surfaces are not thermally protected. Usual anti-icing systems involve heating the leading edge of the airfoil. As they are unable to freeze, the droplets tend to coalesce and form a continuous thin water film. This runback water flows to downstream regions, driven by pressure and shear forces due to the external airflow around the airfoil, and its thickness varies streamwise. When a critical thickness is reached, surface tension effects become dominant, and it is energetically favorable for the film flow to break up into rivulets. The presence of rivulets affects the performance of the anti-icing system because it decreases the effective area of heat and mass transfer between the water, the airfoil surface, and the external airflow. It is therefore fundamental to be able to predict where the water film will break up into rivulets on an airfoil, and which rivulet pattern will be adopted. In this paper, a state of the art of the prediction methods for rivulet transition is presented. An emphasis is first given to the macroscopic Minimum Total Energy model, which is confronted to experimental data for sheared films. A microscopic approach, in which the film and rivulet flows are fully computed, is then presented, based on the film solver of the CFD code OpenFoam[®]. The model is validated for a falling film, and its advantages and drawbacks are emphasized in the perspective of using it for ice accretion applications.

2. State of the art

When subjected to mass forces (gravity or centrifugal), pressure gradients, or shear stress (tangential airflow or surface tension gradient), a continuous liquid film may breakdown in rivulets. This topic covers therefore a broad range of applications, from the most academic test cases (film flowing down an incline plane) to more industrial applications (icing on aerodynamic surfaces, surface cooling in industrial processes...). This literature review starts with the experimental studies of rivulets in simple configurations, such as the film flow down an incline, and the sheared film flow. The different prediction methods are then reviewed in details.

2.1 Experimental approach

A vast majority of experimental studies deal with the film flow down inclined planes subject to gravity only. In this configuration, the advancing contact line is sensitive to transverse perturbations, due to surface irregularities for example, which may perturb the contact angle. Most references deal with constant volume flows, in which a given volume of fluid is released on the surface, and gets thinner with time. This configuration is in essence close to the sheared water film in icing applications, where the thickness decreases in the streamwise direction. We can cite the

PREDICTION OF RIVULET TRANSITION

studies of Silvi and Dussan,³² De Bruyn,⁶ Veretennikov et al.³³ and Hocking et al.¹⁴ These authors underline the existence of two main types of rivulet patterns: with highly wetting fluids, sawtooth rivulets are found, while with partially wetting fluids, they take the shape of fingers with parallel sides. As for constant flux flows, characterized by auto-similar velocity profiles within the film, only one study is reported, from Johnson et al.¹⁶ The authors have developed a Laser Induced Fluorescence technique to reconstruct the full thickness distribution for a falling film, with liquids and surfaces that feature varying contact angles.

As far as sheared films are concerned, the literature is much more scarce, due to the difficulty in generating a continuous liquid film which is sufficiently thin to undergo transition to rivulets. To our knowledge, the only studies dealing with this kind of configuration are the ones of Zhang et al.^{34, 35} in which a water film is generated by the impingement of liquid droplets on a NACA0012 profile in an icing wind tunnel. With a digital image projection technique, they recover the film thickness distribution on the profile, and they demonstrate that the sheared film is actually continuous in the region of the leading edge, before breaking down into rivulets. The quantitative results thus obtained provide an interesting test case and will be used for validation here.

2.2 Theoretical and numerical approach

Various approaches for predicting film breakdown can be reported: macroscopic models aim at computing no more than a wetting factor, which makes them suitable for engineering applications. In microscopic models, the rivulets are explicitly computed through thin-film approximation of the Navier-Stokes equations. In numerical approaches, the 3D flow of both the gas and liquid phases is solved without any approximation. Each method is detailed hereafter.

- Macroscopic modeling

This type of approach aims at estimating a wetting factor, which is the ratio between the wetted surface and the total substrate surface. There is no explicit calculation of the film flow and rivulets. This strategy is based on empirical and simplified considerations, which have never been extensively validated up to now. Yet, it is the only model which has been implemented in ice-accretion and anti-icing codes, due to its negligible computational cost.

The modeling strategy is based on the Minimum Total Energy criterion (later referred to as MTE) to predict the critical film thickness for transition to rivulets, and once breakdown has occurred, the characteristics of rivulets (height and spacing between them). The model considers that under the effect of external forces, the film thins until reaching a critical value h_0 below which capillary effects become dominant. It then becomes energetically favorable for the film to separate in rivulets. In the MTE model developed in section 3.1, it is stated that at film breakdown, the total energy (kinetic+surface tension) and the mass are conserved between the continuous film flow and the rivulet flow. The most stable rivulet pattern is found by minimizing the total energy.

The MTE criterion was initially proposed by Hobler,¹³ and later developed by Mikielewicz et al. for respectively a film flow down an incline²⁶ and a sheared film.²⁵ These authors assume semi-cylindrical rivulets, with a one dimensional velocity distribution. Later, other authors developed more sophisticated models in which the 2D velocity distribution across the rivulet cross section is computed numerically, and the rivulet shape is calculated explicitly instead of making any assumption^{30, 10}. While the MTE model was validated for falling films,²⁶ there was no attempt up to now to validate it for sheared films, because of the lack of experimental data.

In icing applications, Al-Khalil et al.²³ and Lima da Silva et al.²¹ have adopted the simple approach of Mikielewicz et al.²⁵ for the implementation of the rivulet model in their anti-icing codes. While Al-Khalil et al. consider a rectangular section for the rivulets, Lima da Silva et al. make the more realistic assumption of a semi-cylindrical shape. The predictions of their respective codes were confronted to the experimental data of Al-Khalil et al.¹ But due to the low number of experimental data points, and the coupling with heat transfer phenomena, it is difficult to draw any conclusion regarding the improvement of the predictions. There is thus a strong need to validate this macroscopic model in isothermal conditions, and independently from the rest of the code.

- Microscopic modeling: Contact line instability

In microscopic approaches, the film and rivulet flows are explicitly computed, based on thin film approximations. The contact line in an advancing film is known to be sensitive to transversal perturbations. This instability is usually due to the formation of a capillary ridge within the film profile, upstream the contact line. There is an abundant literature on the stability of liquid films down inclined planes. Some authors consider completely wetting fluids^{4, 7, 19, 9}, while others treat partially wetting fluids, using a disjoining pressure to account for molecular phenomena at short distances from the substrate^{22, 8, 11, 12}. In order to overcome the mathematical singularity at

the triple line (the viscous dissipation tends to infinity when the distance to the wall tends to zero), a precursor film is often introduced^{7,19} or a slip condition is developed^{12,29}. It is important to underline that the lubrication assumption is commonly used, even if it clearly ceases to be valid close to the contact line in the case of partially wetting fluids. Kondic and Diez⁸ justify its use by the small differences detected with respect to the predictions of the full Navier-Stokes equations for contact angles smaller than 30°. The computational cost increases considerably when taking into account partial wetting phenomena in the vicinity of the liquid front. It is interesting to note that even in the case of completely wetting fluids, for which the contact angle is virtually null, Kondic and Diez¹⁹ predict rivulet patterns that are surprisingly similar to the experimental observations of Johnson et al.¹⁶ made with weakly wetting mixtures of glycerine and water. The theoretical predictions are obtained by perturbing randomly the liquid front and checking its non-linear evolution at long times. This would mean that the formation of rivulets is not only linked to the partial wetting conditions, but could be triggered by a simple perturbation of the liquid front. This fact remains to be demonstrated experimentally with highly wetting fluids. The scenario of rivulet transition invoked here is rather different than the one developed in the MTE model: the film flux, and thus the film average thickness is constant before transition.

It is worth mentioning an approach in the finite volumes spirit, proposed in the OpenFoam[®] code. The film equations derived from thin-film assumptions are integrated through the film thickness and solved with a finite area method. The later solves the equations on a boundary patch of the volume mesh which is extruded on one cell. The details of the model are developed in section 4. The contact angle effect is introduced with a discrete form of the surface force which comes as a function of the static contact angle. In order to generate rivulet transition, a non-uniform distribution of the contact angle is assumed on the substrate, following the idea of Marshall and Wang²³ who studied rivulet flow in presence of surface contamination. It is interesting to mention the multiphysics solver developed by Kinzel et al.¹⁸ for the prediction of ice accretion, implemented on the basis of the OpenFoam[®] film flow solver. It computes successively the impinging droplet trajectories, the resulting liquid film flow, the film solidification and the ice deformation. In the regions of running wet film, its possible separation in rivulets could therefore be predicted. But the solver has never been validated up to now.

- Numerical modeling

In numerical approaches, the full 3D Navier-Stokes equations are solved, without any approximation. A diphasic solver is generally used, in which one single equation system is solved for both the liquid and gas phase, and one transport equation for the liquid volume fraction α is used to track the position of the interface (Volume of Fluid method). Surface tension effects are accounted for through the Continuous Surface Force Model.⁵ As for the contact angle effects, they are usually taken into account by fixing the angle of the volume fraction α at the wall. With this kind of model, the pinching of a falling film has been successfully predicted^{15,31}. But the full Navier-Stokes approach remains scarcely used due to its important computational cost.

3. Minimum Total Energy model (MTE)

3.1 Model equations

The MTE model consists in a system of 4 equations with 4 unknowns: the critical film thickness for transition h_0 , the rivulet radius R , the center to center rivulet spacing λ and the rivulet wetness factor F_r . As illustrated in figure 1, the later is a wetted area factor defined as the ratio between the rivulet base width and the spacing between two rivulets:

$$F_r = \frac{2R \sin \theta_0}{\lambda} \quad (1)$$

where θ_0 is the contact angle along the rivulet.

The set of equations to be solved consists in the mass conservation between film and rivulet flow in the streamwise direction, the conservation of total energy ($e_t = e_K + e_S$, e_K being the kinetic energy and e_S the surface tension energy) from film to rivulet, the rivulet total energy minimization and geometrical relationships. Assuming a Couette flow velocity profile $v = v(y)$, the mass flow rate per unit width in the film \dot{m}'_f and rivulets \dot{m}'_r is estimated by:

$$\frac{\dot{m}_f}{\lambda} = \dot{m}'_f = \int_0^{h_0} \rho v(y) dy = \frac{\rho \tau}{2\mu} h_0 \quad (2)$$

$$\frac{\dot{m}_r}{\lambda} = \dot{m}'_r = \frac{2}{\lambda} \int_0^{R \sin \theta_0} \int_0^{h(x)} \rho v(x, y) dx dy = \frac{\rho \tau}{\mu} \frac{\phi(\theta_0)}{\lambda} R \quad (3)$$

PREDICTION OF RIVULET TRANSITION

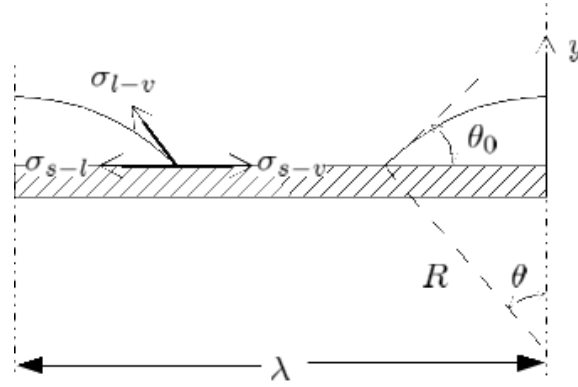


Figure 1: Cross section of rivulets

where τ is the shear stress at the film interface, ϕ and g are functions of θ_0 (see²¹ for their complete expression). The total mechanical energy of the film e_f and of rivulets e_r is given by:

$$\frac{E_f}{\lambda} = e_f = \int_0^{h_0} \frac{\rho}{2} v^2(y) dy + \sigma_{lv} + \sigma_{ls} = \frac{\rho \tau^2}{6\mu^2} h_0^3 + \sigma_{lv} + \sigma_{ls} \quad (4)$$

$$\begin{aligned} \frac{E_r}{\lambda} = e_r = & \frac{\rho}{\lambda} \int_0^{R \sin \theta_0} \int_0^{h(x)} v^2(x, y) dx dy + \left(\frac{2R\theta_0}{\lambda} + \cos \theta_0 - \frac{R \sin 2\theta_0}{\lambda} \right) \sigma_{lv} + \sigma_{ls} = \\ & \frac{\rho \tau^2}{6\mu^2} g(\theta_0) h_0^3 \left(\frac{\sin \theta_0}{\phi(\theta_0)} \right)^{3/2} F_r^{-1/2} + \left(F_r \frac{\theta_0}{\sin \theta_0} + \cos \theta_0 - F_r \cos \theta_0 \right) \sigma_{lv} + \sigma_{ls} \end{aligned} \quad (5)$$

where σ_{lv} and σ_{ls} are the liquid-gas and liquid-solid surface tension. Applying mass and energy conservation, we get the following two equations:

$$R = h_0 \left(\frac{\sin \theta_0}{\phi(\theta_0) F_r} \right)^{1/2} \quad (6)$$

$$h^+ g(\theta_0) \left(\frac{\sin \theta_0}{\phi(\theta_0)} \right)^{3/2} F_r^{-1/2} + \left(\frac{\theta_0}{\sin \theta_0} - \cos \theta_0 \right) F_r - (1 - \cos \theta_0) - h^+ = 0 \quad (7)$$

The most stable rivulet pattern is found by minimizing the rivulet total energy with respect to the wetness factor F_r :

$$\frac{\partial e_r}{\partial F_r} = 0 \quad \text{and} \quad \frac{\partial^2 e_r}{\partial F_r^2} > 0 \quad (8)$$

Combining equations (7) and (8), an equation in terms of adimensional film thickness $h^+ = (\rho \tau^2 h_0^3) / (6\mu^2 \sigma_{lv})$ is found:

$$h^+ = 3 \times 2^{-2/3} \cdot \left(\frac{\theta_0}{\sin \theta_0} - \cos \theta_0 \right)^{1/3} \cdot [h^+ \cdot g(\theta_0)]^{2/3} \cdot \frac{\sin \theta_0}{\phi(\theta_0)} - (1 - \cos \theta_0) \quad (9)$$

Once h^+ is known, h_0 and F_{r0} can be easily deduced, as well as λ and R . The model will now be validated against the experimental data of Zhang et al. for a sheared water film on a NACA profile.

3.2 CFD simulations of the airflow

In the case of a sheared film, one input of the MTE model is the shear stress distribution at the film interface, which is approximated here by the distribution around the airfoil in single phase conditions. For that purpose, several computations are performed around a NACA0012 airfoil with zero angle of attack and for Reynolds numbers ranging between $6,7 \times 10^4$ and $1,7 \times 10^5$, reproducing the experimental conditions of Zhang et al.³⁴ The simulations are run with OpenFoam[®] 2.3.

Beforehand, the solver was validated for a NACA0012 test case at zero angle of attack, and Reynolds number 6×10^6 , for which experimental and numerical data available in literature.²⁸ Structured hexahedral C-type meshes are

used, with respectively 146 000 and 443 000 cells. In order to solve the boundary layer, the first cell height normal to the wall is set at $y = 4 \cdot 10^{-6}$ m, ensuring $y^+ < 1$. The SIMPLE algorithm is used, while a second order upwind scheme is chosen for convective term discretization and limited second order central scheme for the diffusion term. Turbulence is accounted for with a $k - \omega$ SST model. The distribution of the friction coefficient C_f is confronted in figure 2 left, to some reference numerical data²⁸ obtained with a NASA solver CFL3D $k - \omega$. The agreement is excellent, supported by a predicted drag coefficient of $C_D = 0.00805$ very close to the experimental value $C_D = 0.0083$ of Ladson et al.²⁰ It is concluded that the model implemented in OpenFoam[®] can be used with confidence for the computations corresponding to Zhang's experimental data, with a chord length $c = 0.101$ m. A similar set-up was used for the simulations, although it is important to underline that Zhang's experiments³⁵ were performed at $Re_c = 6,7 \times 10^4 - 1,7 \times 10^5$, hence laminar conditions are expected along almost all the chord. This is why the transition model $kkL - \omega$ of Keith et al.¹⁷ is also used here. Nevertheless, the presence of the water film which undergoes surface shear instabilities is probably sufficient to trip turbulence near the leading edge. This justifies the use of the fully turbulent $k - \omega$ SST model. The friction coefficient distributions obtained with the two turbulence models are plotted in figure 2 right, for two meshes of 117 000 ($y^+ \approx 1$) and 235 000 cells ($y^+ < 1$) respectively. Starting from $x/c = 0.15$, we can clearly see the deviation between the $k - \omega$ SST predictions, which are turbulent and attached all along the foil, and the $kkL - \omega$ predictions which show flow separation and transition near the trailing edge, at $x/c = 0.9$. It can be anticipated that the discrepancy between the two models on the first half of the chord will have a non negligible influence on the MTE model because according to Zhang et al.,³⁵ transition to rivulets takes place between $x/c = 0.2$ and 0.4 . It is difficult to assess with certainty the boundary layer regime along the foil in those particular conditions.

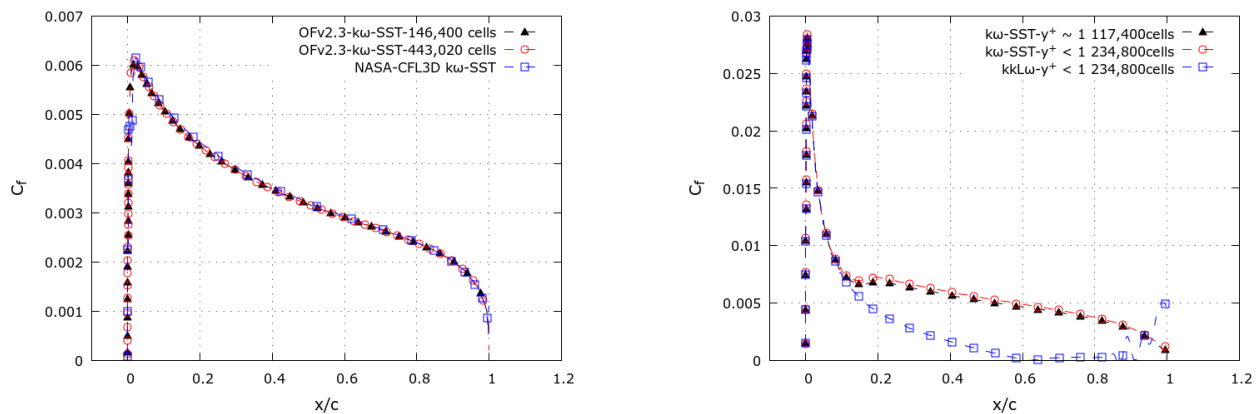


Figure 2: Single phase simulations of the airflow around the NACA0012 profile. Left: Validation test case at $Re_c = 6 \times 10^6$. Right: Test case of Zhang et al.³⁵ at $\alpha = 0^\circ$ and $Re_c = 1.7 \times 10^5$

3.3 Model validation

The shear stress distributions obtained with the $k - \omega$ and $kkL - \omega$ models are now injected in equation (9) to predict the critical film thickness h_0 and the rivulet spacing λ for a water film of surface tension $\sigma = 0.07$ N/m. Since the contact angle of the rivulet is not given by Zhang et al.,³⁵ it is varied between 30 and 60° to study the sensitivity of the model to this parameter. In figure 3, the critical film thickness for transition is represented as a function of the position x/c along the chord. On the same graph, the mean thickness distribution measured by Zhang et al.³⁵ is plotted together with the uncertainty of the measurements estimated at $\pm 20 \mu\text{m}$.

At two different Reynolds numbers, it turns out that the measured thickness is well below the predicted h_0 , which means that transition to rivulets should be immediate. In the experiments of Zhang et al.,³⁵ it seems the film is continuous due to the non stop impingement of droplets near the leading edge. In addition, the average thickness in this region reaches the order of magnitude of the uncertainty. In their anti-icing code, Lima da Silva et al.²¹ consider that even if the critical thickness is reached inside the impingement region, the film does not break down into rivulets due to the effects of multiple droplet impact and spreading. Similarly, transition to rivulets in the predictions of Al-Khalil et al.² is immediate out of the impingement limits. Therefore, it is not inconsistent to predict critical thicknesses lower than the actual values, especially not knowing where the impingement limits of the sprays are located. The optimum rivulet spacing λ is then confronted to the experimental findings of Zhang et al.³⁵ in figure 4. The mean spacing is estimated through digital image processing of the time averaged thickness mappings provided by Zhang et al. A sample image for each condition is added in figure 4. The uncertainty is approximated by the standard deviation of the measurements.

PREDICTION OF RIVULET TRANSITION

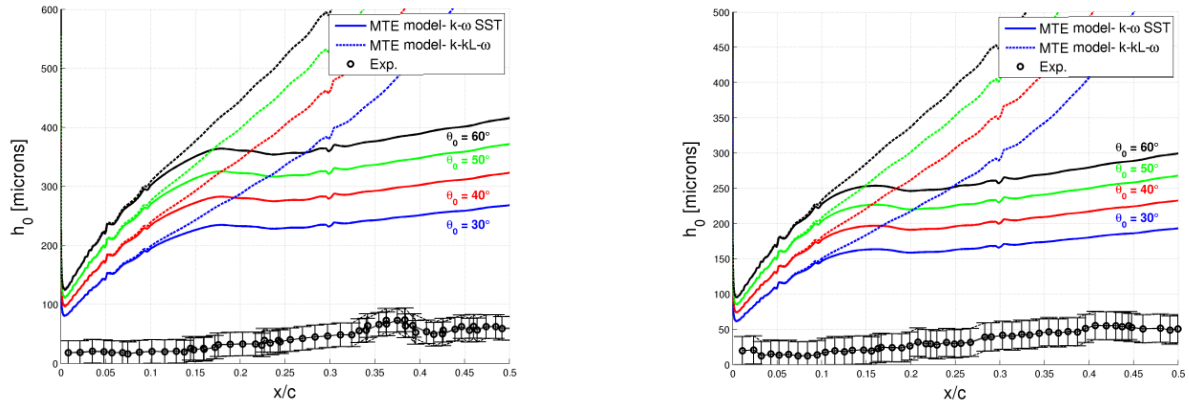


Figure 3: Critical film thickness h_0 predicted by the MTE model for $Re_c = 1.35 \times 10^5$ (left) and $Re_c = 1.7 \times 10^5$ (right)

For both Reynolds numbers, it is found that the experimental points fall within the uncertainty of the predictions, due mainly to the contact angle and boundary layer regime. The order of magnitude of λ is reasonably well predicted, but more data would be needed to validate the model. The process of transition to rivulets is probably different from the one that occurs when a film is thinning, and the influence of droplet impingement cannot be neglected.

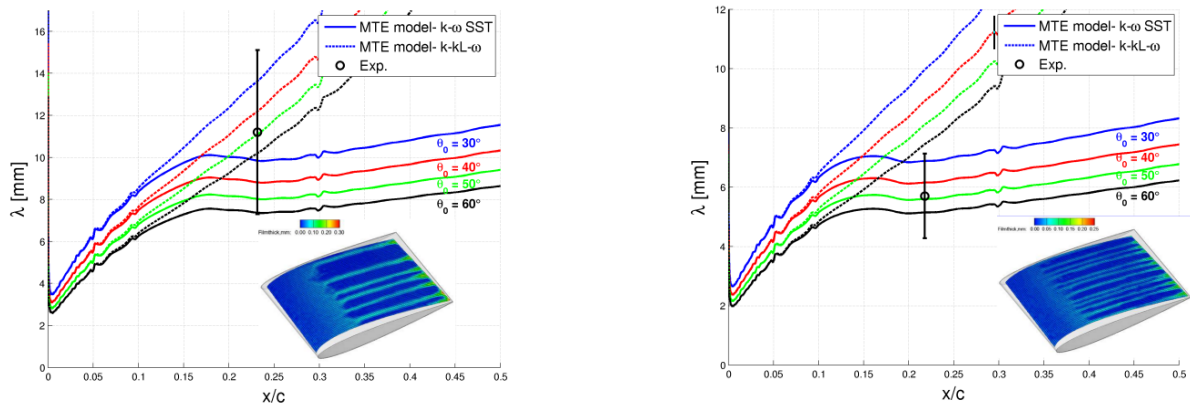


Figure 4: Rivulet spacing λ predicted by the MTE model. for $Re_c = 1.35 \times 10^5$ (left) and $Re_c = 1.7 \times 10^5$ (right). Experimental data from Zhang et al.³⁵

4. Numerical approach with OpenFoam

In a second approach, the film and rivulet flows are completely calculated. The OpenFoam[®] 2.3 solver reactingParcelFilmFlow is used, which allows computing the deposition of droplets on a substrate, the evolution of the resulting liquid film, and its possible separation. The details of this solver are reported in.²⁴ It is composed of:

- an eulerian solver for the gas phase
- a lagrangian solver for droplet motion
- a film solver
- the coupling between the different phases: gas/droplets, gas/liquid film, and droplets/liquid film (stick to wall)

4.1 Equations

The film solver is based on boundary layer type approximations: the tangential derivatives within the film are negligible with respect to the normal ones, the normal velocity is negligible with respect to the tangential one, and the pressure

is constant through the film. This allows integrating the continuity and momentum equations across the film thickness. Both equations are taken in their non-conservative form, with the source terms gathered on the right hand side. The latter represent the gain or loss of mass and momentum due to droplet impingement, splashing, separation, and evaporation. The expression of each of these terms will not be detailed here since they are not relevant for the application considered. The two unknowns of the system are the film thickness h and the film average velocity defined as:

$$\bar{v} = \frac{1}{h} \int_0^h v dh \quad (10)$$

The continuity equation reads:

$$\frac{\partial \rho h}{\partial t} + \nabla_s \cdot (\rho h \bar{v}) = S_{\rho h} \quad (11)$$

where $S_{\rho h}$ is the source term representing the gain or loss of mass due to droplet impact, splashing, evaporation, absorption and separation respectively:

$$S_{\rho h} = S_{\rho h, imp} - S_{\rho h, splash} - S_{\rho h, vap} - S_{\rho h, abs} - S_{\rho h, sep} \quad (12)$$

In the momentum equation (13), the source term is separated into a momentum normal component based on the pressure gradient, and a tangential component $S_{\rho h \bar{v}}$. In the absence of heat transfer, only equations (11) and (13) are used.

$$\frac{\partial \rho h \bar{v}}{\partial t} + \nabla_s \cdot (\rho h \bar{v} \otimes \bar{v}) = -h \nabla_s p + S_{\rho h \bar{v}} \quad (13)$$

where p is the pressure in the liquid:

$$p = p_g + p_h + p_\sigma + p_{imp} + p_{splash} + p_{vap} \quad (14)$$

p_g is the gas pressure, and $p_h = \rho g_n h$ the hydrostatic pressure. In the expression (14), p_σ is the contribution of surface tension given by Laplace equation, in which the interface curvature K is approximated by the laplacian of the thickness (long wave hypothesis):

$$p_\sigma = \sigma K \approx -\sigma \nabla_s^2 h \quad (15)$$

For the other terms, the reader may refer to.²⁴ $S_{\rho h \bar{v}}$ is the tangential momentum source term:

$$S_{\rho h \bar{v}} = \tau_i - \tau_w + g_t h + \tau_\theta + \tau_{Mar} + S_{\rho h \bar{v}, imp} - S_{\rho h \bar{v}, splash} - S_{\rho h \bar{v}, sep} \quad (16)$$

The two first terms represent the shear stress at the film interface and at the wall respectively. For the latter, a quadratic velocity profile is assumed within the film, which yields for the wall shear stress:

$$\tau_w = -\mu \frac{3U}{h} \quad (17)$$

where U is the substrate velocity. The third term is the stress due to thermocapillar effects:

$$\tau_{Mar} = -\nabla_s \sigma \quad (18)$$

The fourth term is the tangential component of gravity, and the last three account for the momentum transfer due to impingement, splashing and separation.

The term τ_θ represents the stress due to the contact angle force that acts along the contact line, and which is non null only for partially wetting fluids. At the contact line, the tangential surface force due to surface tension is expressed per unit length of the contact line as (see figure 1):

$$F_\sigma = \sigma_{l-v} + \sigma_{s-l} - \sigma_{s-v} \quad (19)$$

where σ_{s-v} is the solid-gas surface tension. At the triple line, Young's law states that the forces are balanced at equilibrium, so that:

$$\sigma_{s-v} - (\sigma_{l-v} \cos \theta + \sigma_{s-l}) = 0 \quad (20)$$

where θ is the contact angle at equilibrium. Combining equations (19) and (20), one obtains an expression for the surface tangential force which acts normal to the contact line in the tangential plane per unit length of contact line:

PREDICTION OF RIVULET TRANSITION

$$F_\sigma = \sigma_{l-v}(1 - \cos\theta) \quad (21)$$

This force is then divided by the width of the computational cell Δ_{cell} in the direction normal to the contact line, and then multiplied by the unit vector normal to the contact line.

$$\tau_\theta = \beta \frac{\sigma_{l-v}(1 - \cos\theta)}{\Delta_{cell}} \mathbf{n}_{cell} \quad (22)$$

β is an empirical parameter used to adjust the predictions to the behaviour of films on real substrates. In the case of a film flow down an incline, it is usually adjusted by comparing the predictions of the critical flow rate below which there is transition to rivulets with experimental values. The contact angle force given by (22) applies only along the contact line, which requires determining the position of the latter. For that, a critical thickness h_c below which the film does not exert enough force to overcome the contact angle effects, is defined. Depending on whether the surface is hydrophilic or hydrophobic, different models are used. It is interesting to note that if the film is formed by the continuous impact of droplets, the wetting criterion is relaxed, and the contact line delineation will occur for a thickness equal to a fraction of the critical thickness h_c . The system of equations to be solved is therefore:

$$\frac{\partial \rho h}{\partial t} + \nabla_s \cdot (\rho h \bar{\mathbf{v}}) = 0 \quad (23)$$

$$\frac{\partial \rho h \bar{\mathbf{v}}}{\partial t} + \nabla_s \cdot (\rho h \bar{\mathbf{v}} \otimes \bar{\mathbf{v}}) + \nabla_s \cdot \left(\rho g_n \frac{h^2}{2} \right) + h \sigma \nabla_s^2 h = \tau_i - \tau_w + g_t h + \tau_\theta \quad (24)$$

The film model is solved on a 2D surface mesh discretized in both directions tangential to the substrate, but only one cell thick in the normal direction. The film equations are solved in a segregated fashion via a preconditioned conjugate gradient method. Convective terms are obtained by an upwind scheme, gradient and diffusive terms via a linear scheme. Time discretization is performed via a backwards Euler method. In order to account for partial wetting phenomena, a stochastic distribution of the contact angle is introduced on the substrate surface. In each cell of the mesh, a random value of θ is chosen within a normal distribution characterized by a mean value and a variance and fixed for the duration of the computation. It is this heterogeneous distribution of the contact angle which gives rise to a non uniform flow with rivulets and dry regions.

4.2 Results

Before studying the film breakdown, the steady-state laminar flow along an inclined plane was validated against the Nusselt solution. Sufficiently far from the liquid discharge, the tangential velocity profile can be expressed as a quadratic function of distance from the wall through the film thickness. The mean velocity is obtained by integrating the velocity profile, and expressed as:

$$U_{Nusselt} = \left(\frac{\nu g \sin \beta}{3} \right)^{1/3} Re_f^{2/3} \quad (25)$$

where ν is the kinematic viscosity of the fluid, β the inclination angle of the surface, and $Re_f = 4\Gamma/\mu$ the film Reynolds number with $\Gamma = \rho h \bar{U}$.

The average film thickness is then:

$$h_{Nusselt} = \left(\frac{3\nu^2}{g \sin \beta} \right)^{1/3} Re_f^{1/3} \quad (26)$$

For the computations, the experimental conditions of Murray²⁷ are reproduced, with silicon oil as a working fluid, with the following properties: $\mu=0.02$ Pa.s, $\rho=960$ kg/m³ and $\sigma=0.02$ N/m. The film Reynolds number was varied between 13 and 170, and the plate angle was fixed at 45 ° and 90 °. As it can be seen in figure 5, the predictions of the OpenFoam[®] film model are in reasonable agreement with the Nusselt solution and with experimental data.²⁷

Now that the average film flow is validated, a non-homogeneous distribution of the contact angle θ is introduced in order to trigger transition. It is important to note that the sequence of θ values along the mesh remains the same, whatever the mesh density. This yields a considerable mesh dependency of the results to the mesh density. A new distribution is therefore implemented, which depends only on the spatial coordinates of the domain points. The expression of the latter is inspired by the initial perturbed condition of Diez and Kondic:¹⁹

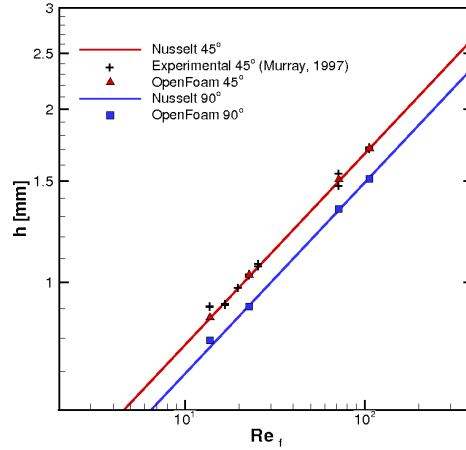


Figure 5: Validation of the mean film thickness on inclined plane with Nusselt theory

$$\theta(x, y) = \theta_0 - \sum_{i=0}^N R_i(\cos(R_{1,i}\pi ix + R_{2,i}\pi iy)), \quad (27)$$

where $R_i, R_{1,i}, R_{2,i}$ are 3 tables of N random transverse mode values, following a standard normal distribution, and where θ_0 is the mean value of the contact angle. With this distribution, the mesh dependence was analyzed with four different mesh densities indicated in table 1, (Ox) being the streamwise direction and (Oy) the cross stream direction.

Table 1: Mesh densities

	Number of cells in (Oy)	Number of cells in (Ox)
Medium	120	240
Intermediate	180	360
Fine	240	480
Extra fine	480	760

In the test case chosen, a flow rate of $\Gamma = 50$ g/m/s of water is flowing down a vertical plate. The properties of water at 20°C are taken as $\nu = 10^{-6} \text{ m}^2/\text{s}$, $\rho = 998 \text{ kg/m}^3$ and $\sigma = 0.078 \text{ N/m}$. According to experimental measurements,²⁴ the equilibrium contact angle of water on plexiglas is about 70°. In the following computations, the average value of θ was fixed at 75°, and its variance at 10°. The empirical coefficient β is fixed at 1, which proves to be a correct value for plates inclined at 90°. Figure 6 shows the thickness distributions obtained with the four meshes. It can be observed that beyond the fine mesh, the results become independent of the grid density, as far as the breakdown position and number of rivulets are concerned. The extra-fine mesh allows capturing in addition the meandering tendency of the rivulets. The number of modes in expression (27) was varied between 20 and 100, as well as the random values of the amplitudes, with a negligible effect on the rivulet pattern. The values of θ_0 and β have more influence, which imposes the validation of the solver for each case.

With the fine mesh, the film flow down an inclined plane at 5° with respect to the horizontal was computed for different flow rates between 50 and 500 g/m/s. The experimental measurements of Meredith et al.²⁴ were used for the validation of this case. As the authors use infrared thermography to visualize the falling film, the working fluid was hot water at 43°C, with the following properties: $\nu = 5,86 \cdot 10^{-7} \text{ m}^2/\text{s}$, $\rho = 990 \text{ kg/m}^3$ and $\sigma = 0.069 \text{ N/m}$. The results presented in figure 7 are obtained with an average contact angle $\theta_0 = 75^\circ$ and a variance of 10°. The critical flow rate for transition to rivulets is best recovered when the β parameter is fixed at 0.4 in this case.

Since the contact angle stress τ_θ (22) that acts along the contact line depends on empirical parameters, it is necessary to analyze the dependence of the results on those parameters: the mean contact angle, its variance, and the β value. The sensitivity of the computations to θ_0 is illustrated in figure 8. It can be observed that decreasing the contact angle leads to a delay in the breakdown of the film: at 65°, the film remains continuous at a flow rate of $\Gamma = 150$ g/m/s, which is in disagreement with experiments. The effect of the contact angle on the pinching of the film is clearly visible. Maintaining a mean contact angle of 75°, the variance of the normal distribution was decreased to respectively

PREDICTION OF RIVULET TRANSITION

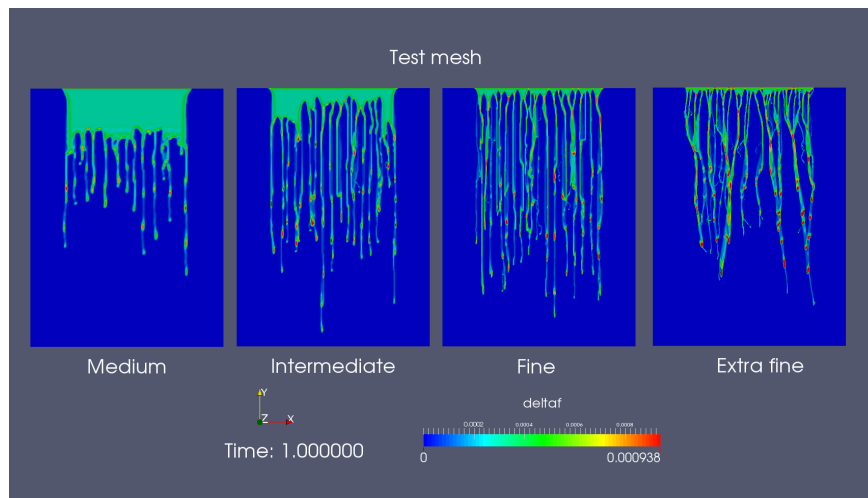
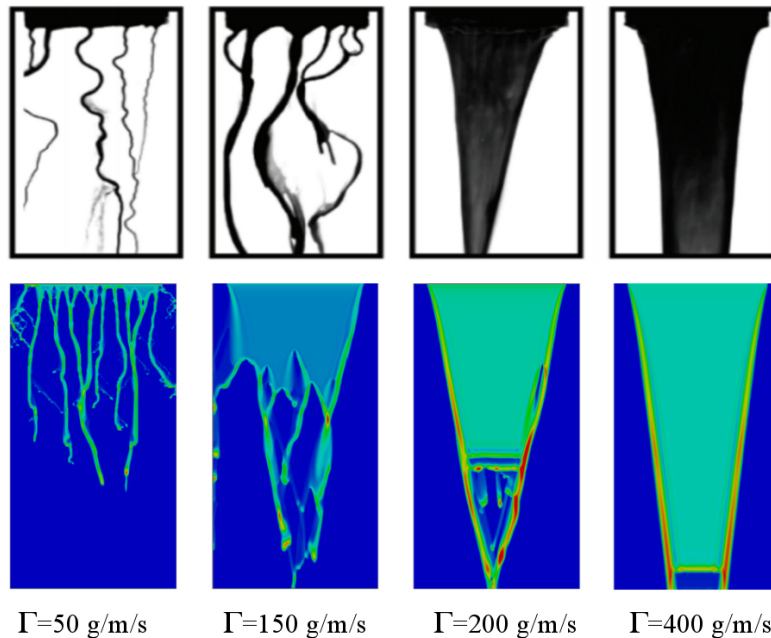


Figure 6: Mesh dependency for a water film on a vertical plate

Figure 7: Falling film on an inclined plane at 5° for different film flow rates. Top: Experimental results.²⁴ Bottom: Predictions of OpenFoam[®] with $\theta_0 = 75^\circ$ and $\beta = 0.4$

5 and 1° in figure 9. The results turn out to be less sensitive to this parameter, since the critical flow rate for film breakdown remains the same. The formation of rivulets is just a little bit different. The importance of the parameter β appears in figure 10, finally. Increasing it from 0.4 to 1 leads to an earlier transition to rivulets, which appears even at the highest flow rate, and which is not consistent with experiments. We also observe an excessive meandering motion of the rivulets, which results in an abnormal coalescence of rivulets for the highest values of β . A correct adjustment of this parameter is thus fundamental to obtain physical results for the falling film. In conclusion, the partial wetting model in this thin film solver is based on highly empirical considerations, which makes it difficult to validate it for a wide range of conditions.

5. Conclusions and perspectives

An extensive review of the methods to predict the breakdown of a liquid film into rivulets is presented in this paper. Among these methods, an emphasis is given to the Minimum Total Energy (MTE) criterion which is a macroscopic model that estimates the wetting factor based on simplified and phenomenological considerations. Although it is the

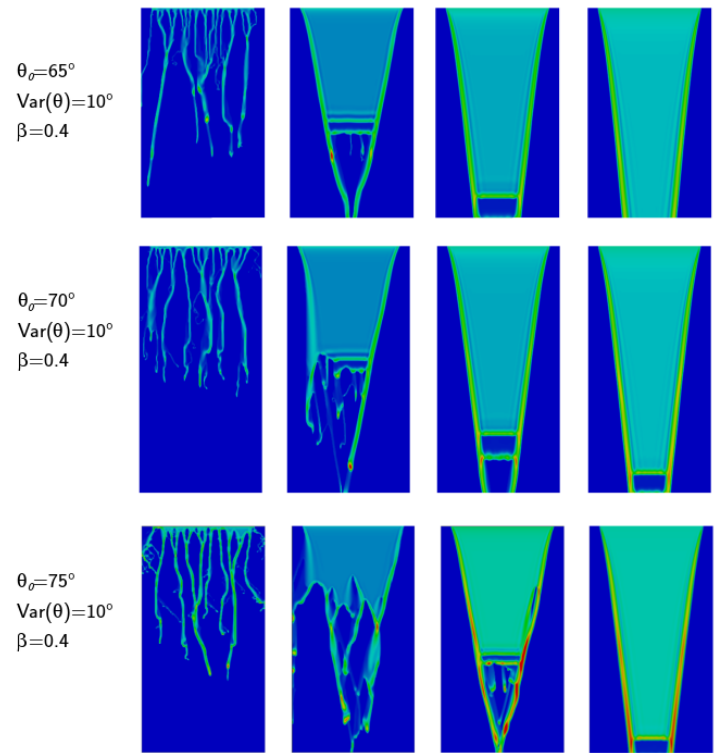


Figure 8: Sensivity of the results to the mean contact angle for different film flow rates between 50 and 400 g/m/s. Variance is fixed at 10° and $\beta = 0.4$

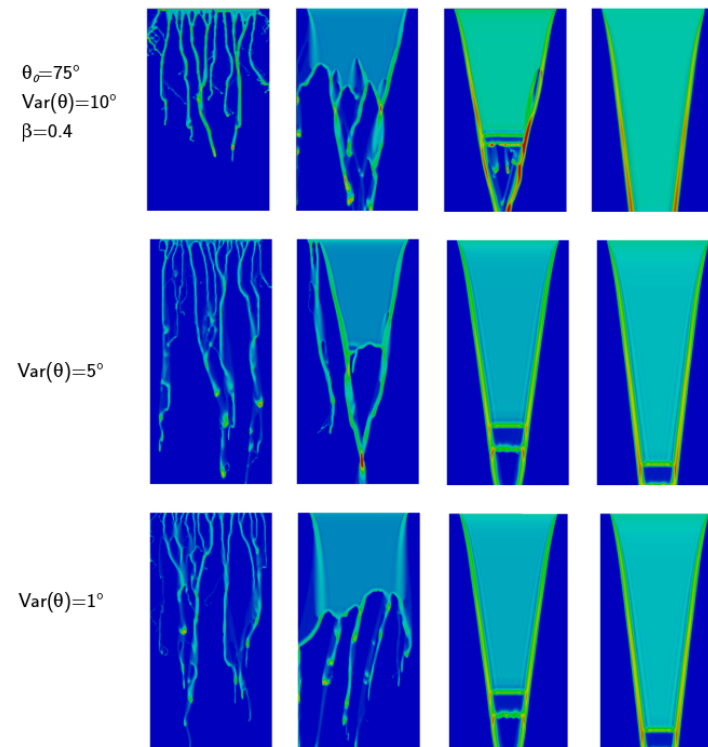


Figure 9: Sensivity of the results to the contact angle variance for different film flow rates between 50 and 400 g/m/s. Mean contact angle is fixed at 75° and $\beta = 0.4$

PREDICTION OF RIVULET TRANSITION

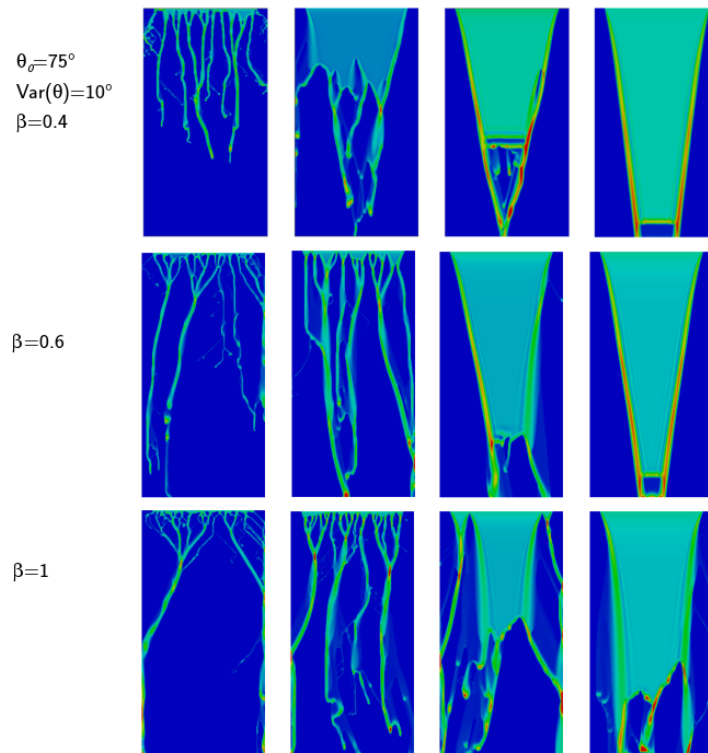


Figure 10: Sensivity of the results to the the empirical parameter β for different film flow rates between 50 and 400 g/m/s. Mean contact angle is fixed at 75° and its variance at 10°

only one implemented in ice-accretion/ anti-icing codes, it has never been validated in isothermal conditions. The MTE criterion is thus applied to a sheared film on a NACA profile and confronted to experimental data from literature. It is found that in typical conditions in which rivulet transition is observed, the film thickness is well below the predicted critical value for breakdown, indicating that the film is continuous only because of the impingement and coalescence of droplets on the substrate. It is thus difficult to validate the MTE model without taking into account the way the film is generated. Regarding the rivulet pattern, the order of magnitude of the spacing between rivulets is in reasonably well predicted, but more data would be needed to confirm the trends. In a second approach, the film and rivulet flow are explicitly computed, based on a thin-film approximation of the Navier-Stokes equations. For that purpose, the film solver developed in OpenFoam[®] is used to compute the breakup of a falling film on an inclined plane. The mechanism to trigger rivulet transition is based on a stochastic distribution of the contact angle on the substrate. It is found that the results are substantially dependent on the mesh density and empirical parameters introduced in the partial wetting model. If the later are correctly calibrated for a particular test case, the critical flow rate for transition is well recovered. The results are mostly sensitive to the mean contact angle and the β parameter. The lack of generality of the model indicates nevertheless that finite contact angle effects should be taken into account in a more physical way, with a disjoining pressure. For anti-icing applications, the basis of the solver remains interesting because it is coupled to an eulerian solver for the gas phase and lagrangian tracking for droplets.

6. Acknowledgments

The technical support of CESGA is gratefully acknowledged, as well as the financial support of ONERA through the Physice 2 convention.

References

- [1] K. M. Al-Khalil, C. Horvath, D. Miller, and W. Wright. Validation of nasa thermal ice protection computer codes. iii-the validation of antice. In *35th Aerospace sciences meeting and exhibit*, page 51, 1997.
- [2] K. M. Al-Khalil, T. G. Keith, and K. J. De Witt. New concept in runback water modeling for anti-iced aircraft surfaces. *Journal of aircraft*, 30(1):41–49, 1993.

- [3] K. M. Al-Khalil, T. G. Keith, and K. J. De Witt. Development of an improved model for runback water on aircraft surfaces. *Journal of aircraft*, 31(2):271–278, 1994.
- [4] A. L. Bertozzi and M. P. Brenner. Linear stability and transient growth in driven contact lines. *Physics of Fluids*, 9(3):530–539, 1997.
- [5] J. U. Brackbill, D. B. Kothe, and C. Zemach. A continuum method for modeling surface tension. *Journal of Computational Physics*, 100(2):335–354, 1992.
- [6] J. R. de Bruyn. Growth of fingers at a driven three-phase contact line. *Physical Review A*, 46(8):R4500, 1992.
- [7] J. A. Diez and L. Kondic. Contact line instabilities of thin liquid films. *Physical Review Letters*, 86(4):632, 2001.
- [8] J. A. Diez and L. Kondic. On the breakup of fluid films of finite and infinite extent. *Physics of Fluids*, 19(7):072107, 2007.
- [9] J. A. Diez, L. Kondic, and A. Bertozzi. Global models for moving contact lines. *Physical Review E*, 63(1):011208, 2000.
- [10] M. S. El-Genk and H. H. Saber. Minimum thickness of a flowing down liquid film on a vertical surface. *International Journal of Heat and Mass Transfer*, 44(15):2809–2825, 2001.
- [11] M. H. Eres, L. W. Schwartz, and R. V. Roy. Fingering phenomena for driven coating films. *Physics of Fluids*, 12(6):1278–1295, 2000.
- [12] R. Goodwin and G. M. Homsy. Viscous flow down a slope in the vicinity of a contact line. *Physics of Fluids A: Fluid Dynamics*, 3(4):515–528, 1991.
- [13] T. Hobler. Minimum surface wetting. *Chemia stosowana B*, 2:145–159, 1964.
- [14] L. M. Hocking, W. R. Debler, and K. E. Cook. The growth of leading-edge distortions on a viscous sheet. *Physics of Fluids*, 11(2):307–313, 1999.
- [15] A. Hoffman, I. Aussner, J.-U. Repke, and G. Wozny. Detailed investigation of multiphase (gas-liquid and gas-liquid-liquid) flow behaviour on inclined plates. *Chemical Engineering Research and Design, Trans. IChemE, Part A*, 84(A2):147–154, 2006.
- [16] M. Johnson, R. A. Schluter, M.J. Miksis, and S. G. Bankoff. Experimental study of rivulet formation on an inclined plate by fluorescent imaging. *Journal of Fluid Mechanics*, 394:339–354, 1999.
- [17] D. Keith Walters and D. Cokljat. A three-equation eddy-viscosity model for reynolds-averaged navier-stokes simulations of transitional flow. *Journal of Fluids Engineering*, 130(12):121401, 2008.
- [18] M. Kinzel, R. Noack, C. Sarofeen, and R. Kreeger. A finite-volume approach to modeling ice accretion. In *28th AIAA Applied Aerodynamics Conference*, page 4230, 2010.
- [19] L. Kondic and J. Diez. Pattern formation in the flow of thin films down an incline: Constant flux configuration. *Physics of Fluids*, 13(11):3168–3184, 2001.
- [20] C. L. Ladson, A. S. Hill, and W. G. Johnson. High reynolds number transonic tests of an naca 0012 airfoil in the langley 0.3-meter transonic cryogenic tunnel. Technical report, NASA, 1987.
- [21] G. Lima da Silva, O. Silvaes, and E. Zerbini. Water film breakdown and rivulets formation effects on thermal anti-ice operation simulation. In *9th AIAA/ASME Joint Thermophysics and Heat Transfer Conference*, page 3785, 2006.
- [22] P. G. López, M. J. Miksis, and S. G. Bankoff. Inertial effects on contact line instability in the coating of a dry inclined plate. *Physics of Fluids*, 9(8):2177–2183, 1997.
- [23] J. S. Marshall and S. Wang. Contact-line fingering and rivulet formation in the presence of surface contamination. *Computers & fluids*, 34(6):664–683, 2005.
- [24] K. Meredith, A. Heather, J. De Vries, and Y. Xin. A numerical model for partially-wetted flow of thin liquid films. *Computational Methods in Multiphase Flow VI*, 70:239, 2011.

PREDICTION OF RIVULET TRANSITION

- [25] J. Mikielewicz and J. R. Moszynski. Breakdown of a shear driven liquid film. *Trans. IFFM*, 66:3–11, 1975.
- [26] J. Mikielewicz and J. R. Moszynski. Minimum thickness of a liquid film flowing vertically down a solid surface. *International Journal of Heat and Mass Transfer*, 19(7):771–776, 1976.
- [27] K. Murray. experimental study of laminar liquid films falling on an inclined plate. Master’s thesis, University of Toronto, 1997.
- [28] NASA. Turbulence model benchmarking working group (tmbwg).
- [29] M. Roux. *Modeles de fronts pour films minces*. PhD thesis, INSA de Toulouse, 2012.
- [30] H. H. Saber and M. S. El-Genk. On the breakup of a thin liquid film subject to interfacial shear. *Journal of Fluid Mechanics*, 500:113–133, 2004.
- [31] D. Sebastia-saez, S. Gu, P. Ranganathan, and K. Papadikis. 3d modeling of hydrodynamics and physical mass transfer characteristics of liquid film flows in structured packing elements. *International Journal of Greenhouse Gas Control*, 19:492–502, 2013.
- [32] N. Silvi and V. Dussan. The rewetting of an inclined solid surface by a liquid. *The Physics of fluids*, 28(1):5–7, 1985.
- [33] I. Veretennikov, A. Indeikina, and H.-C. Chang. Front dynamics and fingering of a driven contact line. *Journal of Fluid Mechanics*, 373:81–110, 1998.
- [34] K. Zhang, B. Johnson, A. P. Rothmayer, and H. Hu. An experimental investigation on wind-driven rivulet/film flows over a naca0012 airfoil by using digital image projection technique. In *52nd Aerospace Sciences Meeting*, page 0741, 2014.
- [35] K. Zhang, T. Wei, and H. Hu. An experimental investigation on the surface water transport process over an airfoil by using a digital image projection technique. *Experiments in Fluids*, 56(9):173, 2015.